Available online at www.sciencedirect.com

ScienceDirect

Procedia Engineering 10 (2011) 3683–3691

Engineering Procedia

Failure analysis of a shaft of a car lift system

D. Crivelli[a], R. Ghelichi[a], M. Guagliano[a,*]

[a]*Politecnico di Milano, Dipartimento di Meccanica - via La Masa 1, 20156 Milano (Italy). Tel: (+39) 0223998206*

Abstract

The failure of a car lift system can result in severe damage to people and structures. It is important to understand the fatigue behavior of these machines, and, in case of a failure, to understand its causes and the possible solutions to increase safety. In this work the failure of the shaft of one of these car lift systems is analyzed. The possible causes of the failure through design, material, fractographical inspections and finite elements analysis were investigated, and possible solutions to avoid these cases in the future are suggested.

Keywords: failure, car elevator, shaft, fatigue, notch effect

1. Introduction and preliminary analysis

Due to the difficulty to find adequate areas for indoor parking in crowded cities, these kind of parkings tend to be developed in the vertical direction. Modern indoor parking areas consist of an elevator system that places the car in a cell in a completely automated way, without the driver on board.

The failure of one of these elevator systems, located in a private block of flats, is analyzed in this work.

The elevator consists of a platform (Figure 1), on which the car is placed by the driver. The platform is moved and supported by a rack-and-pinion system. The platform is placed on two shafts, connected to a motor with a gearbox. It is interesting to note that the gearbox is not centered longitudinally; this makes the torque not well balanced between the two sides of the supporting shaft.

In the studied case the elevator suffered from the breakage of a shaft while loaded, resulting in the failure of the platform on which the car was placed, and consequently the fall of the car which was standing on the platform.

*Corresponding author
Email address: mario.guagliano@mecc.polimi.it (M. Guagliano)

 doi:10.1016/j.proeng.2011.04.606

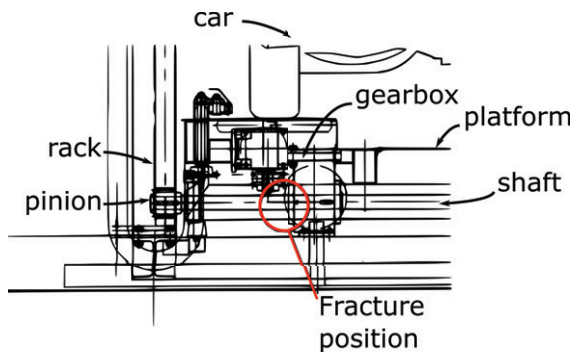

Figure 1: Detail of the elevator platform

Figure 2: Section of the broken shaft with the pinion still mounted

1.1. In-situ visual inspection

Immediately after the failure, a visual inspection at the location of the event was carried out.

The documentation available also proved that the maintenance had been regular. Since the damage was evident (the shaft was split in two parts, see Figure 2), only the two shafts that sustained the platform, along with the gearboxes, were taken away.

All the following tests were carried out in the laboratories of the Mechanical Engineering Department of Politecnico di Milano. Every test was referred to the appropriate guidelines or best practices, where applicable, and performed by certified operators and tools. In particular the X-ray diffraction analyses were referenced to National Physical Laboratory *Determination of Residual Stresses by X-ray Diffraction* [1]; the roughness measurements were according to ISO 4288 [2]; the Magnetic Particle Tests were according to ASTM E1444-05 [3] and ASTM E709 [4].

2. Visual analysis

The shaft broke near the gearbox enclosure. The breaking zone lies near a slot, which is situated in the *short side* of the shaft. The slot is used to fit a seeger ring for the mounting of a gear.

The fractured surface doesn't show noticeable deformations. A very wide shiny zone, typical of fatigue damage, can be seen in Figure 3.

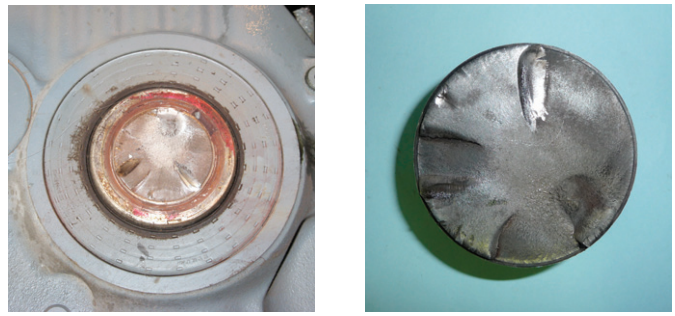

(a) Gearbox side (b) Shaft side

Figure 3: Fracture section surfaces

Table 1: Nominal chemical composition of C45 steel, excluding Fe [7]

C%	Si%	Cr%	Mn%	Ni%
0.42 - 0.50	0.17 - 0.37	< 0.40	0.50 - 0.80	< 0.40

There appear to be multiple crack nucleation points on the outer circumference; this is typical of strong notch effect zones. The final fracture area is small, which leads to the conclusion that the section has been safe (at least statically) regarding applied loads.

3. Metallographic analysis

The shaft material is, according to the manufacturer, a C45 steel. The nominal chemical composition is reported in Table 1.

Two samples from the fracture area were analyzed. The samples were cut from the inner zone and the outer zone of the section.

Both samples were polished, included in resin and chemically etched by a Nital 2% solution, to make the microstructure clear.

Observation on both samples showed a mainly martensitic structure. The chemical composition is reported in Table 2. The Cr levels are unusally high for this material (C45), and include

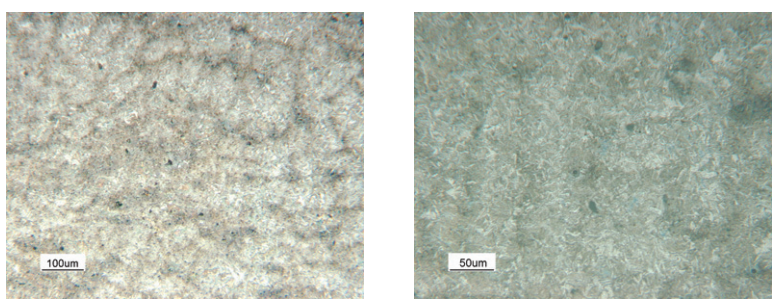

Figure 4: Optical microscope images

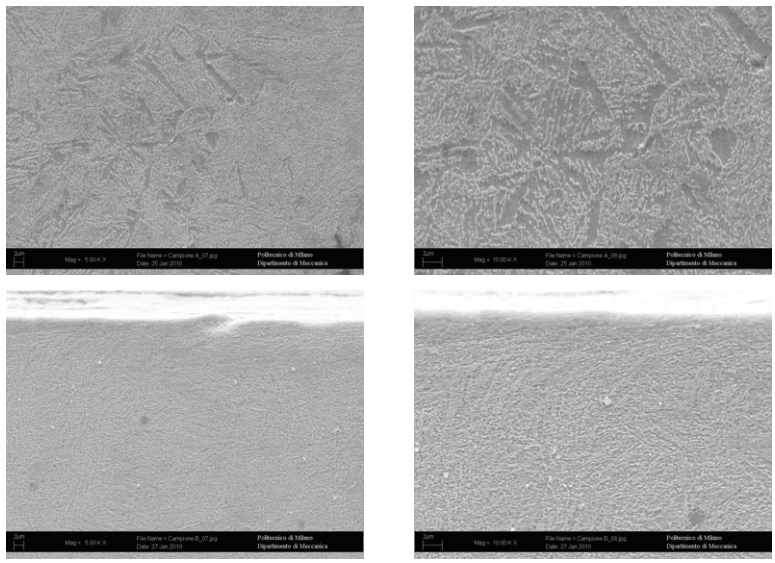

Figure 5: SEM images

Table 2: Chemical composition (weight %. C excluded)

Spectrum	Si %	Cr %	Mn %	Fe %	Ni %	Tot %
1	0.32	0.86	0.89	97.35	0.57	100.00
2	0.29	0.98	0.92	97.27	0.54	100.00
3	0.32	0.93	0.73	97.33	0.69	100.00

(besides Fe and C), also Chromium (1%), Nichel (0.5%). This may indicate that the material was a more performing steel than C45. Additionally, no relevant defects or inclusions were visible.

4. Surface hardness and microhardness measurement

To evaluate the correctness of the thermal treatment of the shaft, some surface microhardness measurements were made.

The measurements were made with a micro hardness tester with a 50g weight near the surface of the B specimen in two different positions. The results are represented in Figure 6.

The hardness tests confirm the results of the chemical analysis, leading to think that this steel has an ultimate strength of about 900-1000MPa.

5. Residual stress analysis

A residual stress measurement was made. Four measurements were made with an AST X3000 X-ray diffractometer, with a circular spot, using 11 angles (5 positive, 5 negative, and 0°position). A circular 2mm^2 spot was used. Each measurement was repeated in three directions

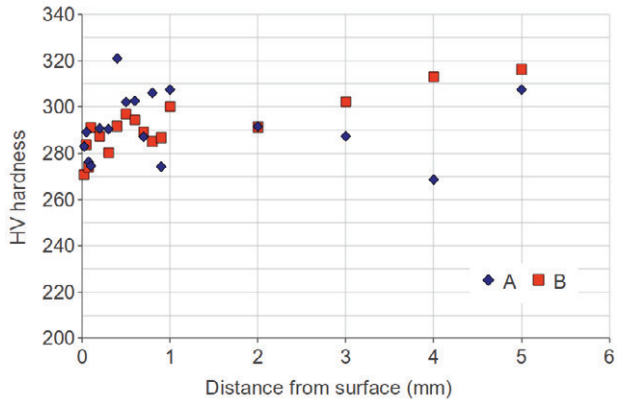

Figure 6: Microhardness tests on sample B, positions A and B

Table 3: Results of the diffractometric analysis: residual stresses

Pos	Stress 0°	Stress 45°	Stress 90°	σ_2	σ_1	φ
1	-219 ± 17	-96.6 ± 13	-2 ± 21	-1	-220	3
2	-201 ± 15	-113.6 ± 15	14 ± 20	-16	-203	5
3	-200 ± 32	-143.1 ± 10	-17 ± 23	-11	-207	-10
4	-286 ± 16	-174.2 ± 11	49 ± 17	-49	-286	-1

(0°, 45°, 90°), where the 90°angle matched the longitudinal axis of the shaft. The cathode used in the measurements was a Chromium cathode. The measurements were made according to NPL's XRD Manual [1].

The diffraction peaks were determined with the cross-correlation method. The exposure time was set to 15s for each angle. The RX signal was recorded by two PSD sensors, which were calibrated before the experiment. The results are reported in Tables 3 and 4.

Measurements reflected an uniform distribution of the residual stresses. σ_1 and σ_2 are the principal stresses, which are calculated from the measured stresses at 0°, 45°, 90°. ϕ is the angle of the principal stress σ_1 from the reference axis (0°).

A graph of the principal stresses can be found in Figure 7. The measurements showed a good definition of diffraction peaks and a reduced scatter, in both stress and peak amplitude.

The principal stress direction is mainly in the machining direction (turning), in the tool cut-

Table 4: Results of the diffractometric analysis: full width half maximum amplitude

Pos	FWHM 0°	FWHM 45°	FWHM 90°
1	3.415 ± 0.025	3.341 ± 0.021	3.339 ± 0.036
2	3.390 ± 0.020	3.336 ± 0.025	3.349 ± 0.054
3	3.406 ± 0.019	3.306 ± 0.024	3.314 ± 0.038
4	3.380 ± 0.028	3.353 ± 0.023	3.285 ± 0.038

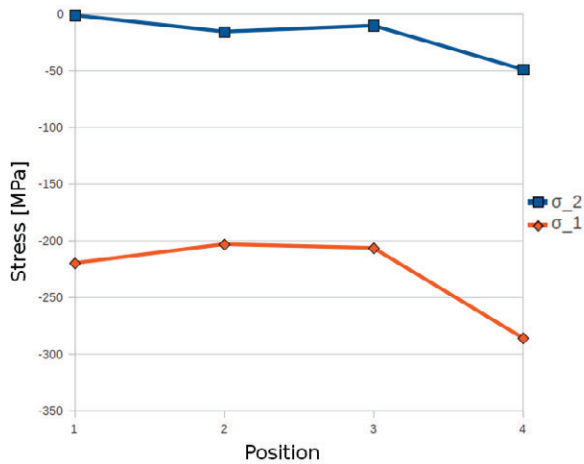

Figure 7: Residual principal stresses σ_1 and σ_2 on the sample

Table 5: Results of the roughness measurements on the sample in μm

Generatrix	R_a	R_q	R_z	R_{max}
0°	4.45	5.29	18.47	19.43
90°	4.36	5.22	18.99	21.05
180°	4.37	5.14	18.00	20.12
270°	3.93	4.78	17.09	20.85

ting direction the stresses are compressive and with an amplitude which is coherent with the machining method. The σ_2 stress is negligible. Since the stresses are compressive they are considered not dangerous.

6. Surface roughness analysis

The instrument used is a Mahr PGK connected to a PCMESS acquisition system and evaluated with the software Perthometer Concept. The pickup used is a Mahr MFW-250 model with a 6851804 arm (stylus tip radius 2μm). The measurement range was set to ±250μm with a wavelength cutoff of 0.8mm. The speed was set to 0.5mm/s. The proof was made in accordance to ISO 4288 [2].

The surface roughness can be a source of crack initiation points. Therefore, we measured the roughness of the same sample we used in the diffractometric tests. We measured the roughness along 4 generatrices along the shaft axis. The results are reported in Table 5.

The R_a roughness is quite uniform and below the design value (which was 12 μm), although there are local high values of roughness (as denoted by the values of R_z and R_{max}) which are quite uniform on the circumference. That could be an indicator of a local bad finishing.

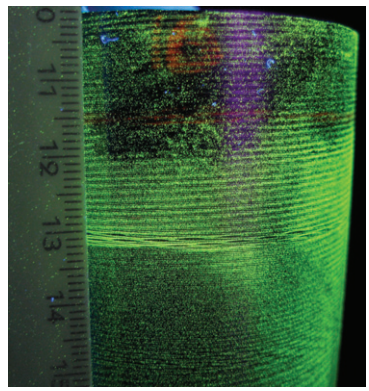

Figure 8: MPI inspection: signal of a turning problem

7. Magnetic particle inspection (MPI)

To investigate the presence of other surface or sub-surface cracks in other zones of the shaft, we analyzed the entire short side of the broken shaft with MPI.

The inspection was made according to ASTM E1444-05 *Standard Practice for Magnetic Particle Testing* [4]. Before the exam the shaft's painted coating was removed accurately with a non aggressive paint remover.

We used fluorescent green magnetic wet particles, applied with a spray can. A magnetic field was applied during the spraying with a magnetic yoke. In the dark room, under UV light (with a Wood Lamp), the particle disposition on the specimen was visible.

During this inspection no fracture was found. However the particles highlighted that the surface roughness degrades in the direction of the gearbox, and a signal of problems during the turning of the shaft was found (Figure 8).

8. Fractographic analysis

We analyzed the fracture surfaces at a electron microscope (SEM). The fractographic analyses evidenced the presence of multiple surface crack initiation points, due to a severe stress intensification factor. The sudden breakage zone is small, as said before. In Figure 9 the crack initiation points can be noticed, and the breakage zone has a ductile aspect. Also, no signs of corrosion were found, neither in the surface nor in the crack initiation points.

9. Analytical strength assessment

For the final check of the shaft the stress concentration of the notches has been calculated based on Peterson [6] stress concentration for different notches. Even if the loading conditions in Peterson book are not for mixed loading (as this case), it can be a good estimation to show the overall situation of the shaft.

Each notch was studied with a classical approach: the moment and torsion on each section and the Mises stress were calculated basing on Peterson Stress Concentration Factors.

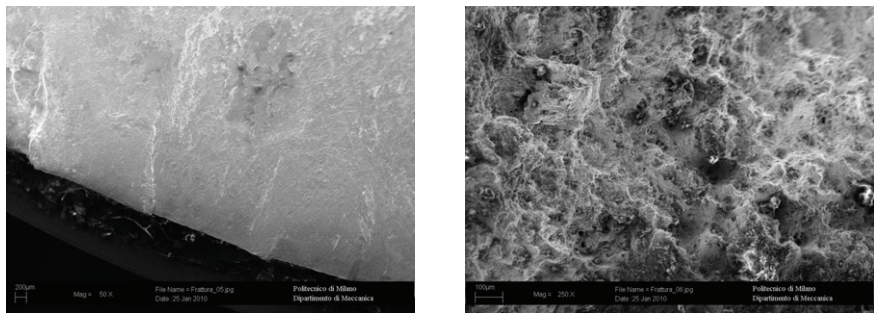

Figure 9: SEM fracture surface images

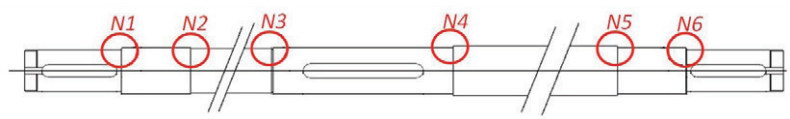

Figure 10: Notch references

Using the results of the analytical model we calculated the fatigue safety factor for each notch. We didn't consider the torsional stress because its effect was negligible.

The fatigue limit was calculated for each notch according to (1):

$$\sigma'_{fa} = \sigma_{fa} \frac{b_2 b_3}{k_f} \tag{1}$$

where σ_{fa} is the fatigue limit of the material (300MPa), b_2 is the geometrical factor (0.9 for this size and material) and b_3 is the roughness factor (0.6 for normal turning). k_f was calculated for each notch according to Peterson and to (2).

$$k_f = 1 + q(k_t - 1) \tag{2}$$

$$q = \frac{1}{1 + \sqrt{\rho}/\sqrt{r}} \tag{3}$$

Results for each notch are reported in Table 6.

It is clear that N1, N2 and N3 have an insufficient safety margin on fatigue.

10. Conclusions

From the analyses it can be deduced that the fracture developed in a section that presents a very high stress concentration factor. and is the most critical zone of the shaft. There were neither microstructural defects or anomalies, nor surface defects, and the chemical analysis of the material shows abnormal alloy elements for the C45-grade steel, which can be typical of a more performing steel (that was confirmed from the hardness tests). The surface of the shaft shows some anomalous turning passages.

Table 6: Fatigue safety margins

Notch	Mises stress (MPa)	k_f(bending)	σ'_{fa}	safety
N1	188	2.20	73.77	0.9
N2	169	1.64	98.54	0.99
N3	138	2.58	62.73	1.24
N4	84	2.17	74.71	2.01
N5	94	2.08	78.02	1.8
N6	80	2.20	73.77	2.12

The failure mode is compatible with the design and applied loads and is strictly related to the severe notch effect in the critical section.

We also proposed some corrective actions to avoid such failures, to be verified during the re-design process: modification of the geometry of the critical section. in particular by removing or smoothing the slot; modification of the turning process parameters, ensuring a more uniform surface roughness of the shaft; execution of a surface treatment to increase the fatigue life of the component, such as shot peening or induction hardening.

Due to the inability to know the exact loading condition and spectra for the lifespan of this kind of systems, we also suggested to adopt adequate safety margins in order to be safe regarding unpredicted loads.

References

[1] National Physical Laboratory, *Determination of Residual Stresses by X-ray Diffraction*
[2] ISO 4288, *Geometrical Product Specifications (GPS) - Surface texture: Profile method - Rules and procedures for the assessment of surface texture*
[3] ASTM E1444-05, *Standard Practice for Magnetic Particle Testing*
[4] ASTM E709, *Standard Guide for Magnetic Particle Testing*
[5] T. L. Anderson, *Fracture Mechanics: Fundamentals and Applications*, CRC Press 1995
[6] Walter D.Pilkey, Deborah F.Pilkey *Peterson's Stress Concentraton Factors*, third edition, John Whiley & sons, 200
[7] George S. Brady et al., *Materials handbook*, McGraw-Hill, 2002